Letter

Self-localized topological states in three dimensions

Rujiang Li [1,*,†] Pengfei Li [2,3,†] Yongtao Jia,[1] and Ying Liu[1,‡]

[1] *Key Laboratory of Antennas and Microwave Technology, School of Electronic Engineering, Xidian University, Xi'an 710071, China*

[2] *Department of Physics, Taiyuan Normal University, Jinzhong 030619, China*

[3] *Institute of Computational and Applied Physics, Taiyuan Normal University, Jinzhong 030619, China*

(Received 22 November 2021; revised 20 April 2022; accepted 6 May 2022; published 18 May 2022)

Three-dimensional (3D) topological materials exhibit much richer phenomena than their lower-dimensional counterparts. Here, we propose self-localized topological states (i.e., topological solitons) in a 3D nonlinear photonic Chern insulator. Despite being in the bulk and self-localized in all 3D, the topological solitons at high-symmetry points K and K' rotate in the same direction, due to the underlying topology. Specifically, under the saturable nonlinearity the solitons are stable over a broad frequency range. Our results highlight how topology and nonlinearity interact with each other and can be extended to other 3D topological systems.

DOI: 10.1103/PhysRevB.105.L201111

Introduction. Since the discovery of the quantum Hall effect and its topological interpretation, extensive efforts have been put into the research of exotic topological materials [1,2]. Dimensionality plays a key role in the classification of topological materials and determination of the topological states [3–5]. Since for a realistic material three is the largest number of spatial dimensions in which electrons can move, three-dimensional (3D) topological materials including Weyl semimetals, 3D topological insulators, and 3D Chern insulators gain particular attention [6,7]. In recent years, various engineered systems have been implemented as the classical analogs of 3D topological materials [8–16]. Among them, 3D photonic topological materials support robust photonic propagation along a nonplanar surface, which may find applications in topological lasers and photonic circuits [8–10]. In these studies, the interaction between photons is neglected.

In topological photonics, it is straightforward to include interparticle interactions. Under high intensity, photons can effectively interact in a nonlinear optical medium with an intensity-dependent refractive index. Several forms of nonlinear refractive indices such as Kerr nonlinearity, competing nonlinearity, and saturable nonlinearity exist [17], and they provide a fertile ground to study the interplay between topology and nonlinearity. Nonlinear topological photonics arises with many opportunities for fundamental discoveries and new functionalities for photonic devices [18]. However, the vast majority of research is carried out in lower dimensions. The studies of 3D photonic topological materials with nonlinearity acts on all three spatial dimensions are rare.

In this Letter we propose self-localized topological states (i.e., topological solitons) which are solely induced by the nonlinearity in a 3D photonic Chern insulator. The 3D Chern insulator is realized by stacking 2D Chern insulators in the vertical direction [7]. In the linear regime (low optical intensity), the 3D Chern insulator supports 2D surface states with chiral propagation along the surfaces, while for the topological states that we discovered in the nonlinear regime, they are self-localized in the bulk of the Chern insulator, rather than localized on the exterior or extended in the vertical direction. Due to the same underlying topology that is shared with the linear surface states, the topological solitons reside in the linear bulk band gap and solitons at the high-symmetry points K and K' rotate in the same direction. Specifically, under saturable nonlinearity, topological solitons are dynamically stable for a wide frequency range.

Our topological solitons in 3D differ from previously reported solitons in lower-dimensional topological materials. First, our topological solitons are self-localized in the bulk. They are fundamentally different from the edge solitons which are localized at the structure exterior or domain wall due to the bulk-boundary correspondence of their linear host lattices [19–25]. Second, our topological solitons are also different from the bulk solitons [26–31]. In the linear regime, by stacking 2D Chern insulators into a 3D Chern insulator, the chiral edge states change into chiral surface states which are extended in the stacking direction. In the nonlinear regime, the introduction of another spatial dimension usually leads to soliton stripes [17]. Our topological solitons are self-localized also in the vertical direction, where interlayer coupling is delicately compensated by nonlinearity. The principle is similar to the balance between diffraction and nonlinearity in the propagation direction of an edge soliton [19,21,23,24]. Such self-localization is important for constructing diffraction-free topological states in 3D topological materials and designing 3D topological photonic devices.

Hamiltonian. We start from a general Hamiltonian

$$H_L = \left(v_0\delta k_z + v_0'\delta k_z^2\right)\sigma_0 + v_x\delta k_x\sigma_1 + v_y\delta k_y\sigma_2 + \left(v_z\delta k_z + v_z'\delta k_z^2\right)\sigma_3 + m\sigma_3, \tag{1}$$

*rujiangli@xidian.edu.cn

†These authors contributed equally to this work.

‡liuying@mail.xidian.edu.cn

where σ_0 is the identity matrix, σ_i ($i = 1, 2, 3$) are Pauli matrices, m is the effective mass, $\nu_{x(y)}$ is the group velocity in the $x(y)$ direction, and $\nu_{0,z}$ and $\nu'_{0,z}$ are the group velocity and group velocity dispersion (GVD) in the z direction, respectively. When $\nu'_0 = \nu'_z = 0$ and $m = 0$, this Hamiltonian reduces to a typical Weyl Hamiltonian [6]. Based on the Weyl Hamiltonian, first we include the GVD terms with δk_z^2 which are necessary to study the nonlinear effect. Specifically, when $\nu_0 = \nu_z = 0$ the second-order contributions need to be considered. The resulting Hamiltonian corresponds to a semi-Weyl point with linear dispersions in the x and y directions, and quadratic dispersion in the z direction (similar to the semi-Dirac point or hybrid Dirac point [32–34]). Then we introduce the mass term m which opens a band gap at the nodal point. Usually, a mass term can be created by breaking the time-reversal symmetry and/or inversion symmetry [35].

Transforming to position space [28], the Hamiltonian is

$$H_L = -i\sigma_0\left(\nu_0\partial_z - i\nu'_0\partial_z^2\right) - i\nu_x\sigma_1\partial_x - i\nu_y\sigma_2\partial_y - i\sigma_3\left(\nu_z\partial_z - i\nu'_z\partial_z^2\right) + m\sigma_3, \tag{2}$$

with $i\partial_t\Psi = H_L\Psi$ and $\Psi = (\psi_A, \psi_B)^T$. We can extend the system into the nonlinear regime by adding a general nonlinear term $H_{\rm NL} = N_0(\Psi)\sigma_0 + N_z(\Psi)\sigma_3$ with $N_{0,z} \in C(\mathbb{R})$ and $N_{0,z}(0) = 0$ to the original Hamiltonian, and the second term $N_z(\Psi)$ is equivalent to a nonlinearity-induced mass. The whole Hamiltonian is $H = H_L + H_{\rm NL}$, and it can be split into two parts $H = H_\parallel + H_z$ with

$$H_\parallel = -i\nu_x\sigma_1\partial_x - i\nu_y\sigma_2\partial_y + m\sigma_3 + N_z(\Psi)\sigma_3, \tag{3}$$

$$H_z = -i\sigma_0\left(\nu_0\partial_z - i\nu'_0\partial_z^2\right) - i\sigma_3\left(\nu_z\partial_z - i\nu'_z\partial_z^2\right) + N_0(\Psi)\sigma_0. \tag{4}$$

Using the Hamiltonian $H_\parallel$, we get a generalized nonlinear Dirac equation. In the special case where $N_z(\Psi) = N_z(\Psi^\dagger\sigma_3\Psi)$, the Gross-Neveu/Soler type of nonlinear Dirac equation supports the Dirac solitons, which are topological solitons in 2D [29,36,37]. The Hamiltonian H_z also admits the existence of solitons in the z direction, provided that the interlayer coupling governed by ∂_z^2 is balanced with the nonlinear term $N_0(\Psi)$ [17]. This principle has been used to realize the edge solitons [19,21,23,24]. Thus, the whole Hamiltonian H should support topological solitons that are self-localized in all 3D.

Lattice model. We study the tight-binding lattice model of a 3D photonic Chern insulator, which is constructed by AA stacking 2D Haldane honeycomb lattices in the vertical direction [38] and introducing interlayer hopping [39] [Fig. 1(a)]. The on-site frequencies at sublattice sites A and B (orange and purple spheres) are $\omega_{A,B}$, respectively. In the xy plane, the nearest-neighbor (NN) hopping (black lines) is t_1, and the next-nearest-neighbor (NNN) hoppings (orange and purple arrows) are $t_2e^{\pm i\phi}$. In the z direction, the interlayer hoppings for sublattice sites A and B are t_A (orange lines) and t_B (purple lines), respectively. The lengths of the nearest-neighbor bonds in the xy plane and z direction are a_0 and h, respectively. In the linear regime, the Hamiltonian of this 3D photonic Chern insulator is $H_L = \sum_{i=0,1,2,3} d_i\sigma_i$, where

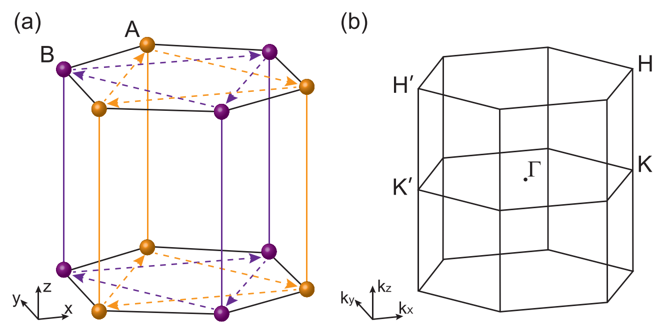

FIG. 1. (a) A 3D Chern insulator constructed by AA stacking the 2D Haldane honeycomb lattices. The orange and purple spheres denote sublattice sites A and B, respectively. In the xy plane, the black solid lines represent the NN hopping t_1, and the orange and purple arrows represent the NNN hopping $t_2\exp(\pm i\phi)$. The orange and purple lines represent interlayer hoppings t_A and t_B, respectively. (b) Brillouin zone of the 3D Chern insulator.

$d_0 = \frac{\omega_A+\omega_B}{2} + (t_A + t_B)\cos(k_zh) + 2t_2\cos\phi\sum_{i=1,2,3}\cos(\mathbf{k}\cdot\mathbf{v}_i)$, $d_1 = t_1\sum_{i=1,2,3}\cos(\mathbf{k}\cdot\mathbf{e}_i)$, $d_2 = -t_1\sum_{i=1,2,3}\sin(\mathbf{k}\cdot\mathbf{e}_i)$, and $d_3 = \frac{\omega_A-\omega_B}{2} + (t_A - t_B)\cos(k_zh) - 2t_2\sin\phi\sum_{i=1,2,3}\sin(\mathbf{k}\cdot\mathbf{v}_i)$. The two sets of vectors $\mathbf{e}_{1,2,3}$ and $\mathbf{v}_{1,2,3}$ are defined for the NN hopping and NNN hopping in the horizontal plane, respectively. Since we are interested in a 3D Chern insulator where the bulk bands are characterized by a triad of Chern numbers $C = (C_x, C_y, C_z) = (0, 0, 1)$, in the following we let $\omega_A = \omega_B$, $t_A = t_B > 0$, and $\phi = \pi/2$. Along the KH and $K'H'$ lines in the Brillouin zone (BZ) [Fig. 1(b)], this 3D photonic Chern insulator has linear dispersions in the horizontal plane with $d_1 = \mp v_F\delta k_x$, $d_2 = -v_F\delta k_y$, and $d_3 = \pm 3\sqrt{3}t_2$ according to $\mathbf{k}\cdot\mathbf{p}$ theory ("−" for KH and "+" for $K'H'$). Now the mass term is solely induced by the NNN hopping, which breaks the time-reversal symmetry. Here, the group velocity v_F is defined as $v_F = \frac{\sqrt{3}}{2}t_1a$ with the transverse lattice period $a = \sqrt{3}a_0$. To study the dispersion in the vertical direction, we focus on the four high-symmetry points, K, K', H, and H', since near these points the first-order contributions are zero. From $d_0 = \frac{\omega_A+\omega_B}{2} \pm (t_A + t_B)(1 - \frac{h^2}{2}\delta k_z^2) - 3t_2\cos\phi$ ("+" for K and K', and "−" for H and H'), this 3D photonic Chern insulator has a quadratic dispersion in the vertical direction. Specifically, it has anomalous GVDs at K and K', and normal GVDs at H and H'. Now the Hamiltonian H_L with $d_{0,1,2,3}$ resembles the Hamiltonian in Eq. (1), except that the eigenfrequency ω is shifted by $\frac{\omega_A+\omega_B}{2}$.

Transforming the Hamiltonian H_L into position space, we add a saturable nonlinear term $H_{\rm NL} = {\rm diag}[N(\psi_A), N(\psi_B)]$ to H_L, where $N(\psi_{A,B}) = g|\psi_{A,B}|^2/(1 + \sigma|\psi_{A,B}|^2)$ with the nonlinear parameter g, saturation coefficient σ, and two pseudospin components $\psi_{A,B}$. Here, we only focus on the self-focusing nonlinearity with $g > 0$ (the case of self-defocusing nonlinearity with $g < 0$ can be studied similarly [40]). The existence of bright solitons requires anomalous GVDs in the vertical direction [17], which are fulfilled only at K and K'. Thus, the whole Hamiltonian is

$$H = \sum_{i=0,1,2,3} \sigma_i d_i, \tag{5}$$

where

$$d_0 = \frac{\omega_A + \omega_B}{2} + t_A + t_B + \frac{t_A + t_B}{2} h^2 \partial_z^2 + \frac{N(\psi_A) + N(\psi_B)}{2}, \tag{6}$$

$$d_1 = \pm i v_F \partial_x, \tag{7}$$

$$d_2 = i v_F \partial_y, \tag{8}$$

$$d_3 = \pm 3\sqrt{3} t_2 + \frac{N(\psi_A) - N(\psi_B)}{2}. \tag{9}$$

Here, "±" correspond to K and K', respectively. Note that this Hamiltonian can also be derived directly from the coupled equations in position space [40].

Similar forms of the Hamiltonian have been studied in free-space Bose-Einstein condensates (BECs) with spin-orbit coupling (SOC), where the SOC terms are analogous to the linear dispersions in the xy plane [41]. However, in contrast to the externally imposed SOC, the linear dispersions are inherent in our lattice model. We only study the fundamental solitons since the higher-order solitons are usually unstable [36], and the parameters are $\omega_A = \omega_B = 10$, $t_1 = 2/\sqrt{3}$, $t_2 = 1.05/3\sqrt{3}$, $t_A = t_B = 0.5$, $a = 1$, $h = 1$, $g = 1$, and $\sigma = 10$. The topological solitons reside spectrally in the topological band gap created by the linear bulk bands. Figures 2(a1)–2(b2) show the two pseudospin components $\psi_{A,B}$ for the topological solitons at K with $\omega = 10$. For the sake of clarity, parts of the isosurfaces are removed. From the isosurfaces [Figs. 2(a1) and 2(b1)], in the horizontal plane the pseudospin component ψ_A features a hump at a nonzero radius, and the component ψ_B decreases monotonously in the radial direction. This behavior of our topological solitons is different from the soliton profile in a Soler model [29], but they share the same origin that nonlinearity induces a mass inversion and creates a topological domain wall in the bulk [26–29,31,40], while in the z direction, the topological solitons are self-localized because of the balance between interlayer coupling and nonlinearity. From the phase distributions on the isosurfaces [Figs. 2(a2) and 2(b2)], a vortex torus carrying a vorticity of $l_A = -1$ is formed for the pseudospin component ψ_A, and the isosurface for ψ_B is a sphere with a zero vorticity, namely $l_B = 0$. The vorticity (or topological charge) is defined as $l_{A,B} = (1/2\pi)\oint_L \nabla[\arg(\psi_{A,B})] \cdot d\vec{l}$. Thus, the topological solitons here are semivortex types [42]. Different from the semivortex BEC solitons which are replaced by the Townes solitons in the absence of SOC [43], our topological solitons vanish when the linear dispersion terms are mathematically removed.

In Figs. 2(c1)–2(d2) we show the topological solitons at the high-symmetry point K' with $\omega = 10$. For a 3D Chern insulator with time-reversal symmetry breaking (inversion symmetry is preserved), d_3 has an opposite sign at K' compared with the value of d_3 at K. This leads to the equal Berry curvatures Ω at K and K', i.e., $\Omega(\mathbf{k}) = \Omega(-\mathbf{k})$, which indicates a nonzero Chern number C_z [38]. Due to the same underlying topology, according to the Hamiltonian H in Eqs. (5)–(9), if we make transformations $\psi_A \to -\psi_B$ and $\psi_B \to \psi_A$ to the equations at K, we can get the equations at K'. From the figures, the component ψ_A has a zero vorticity

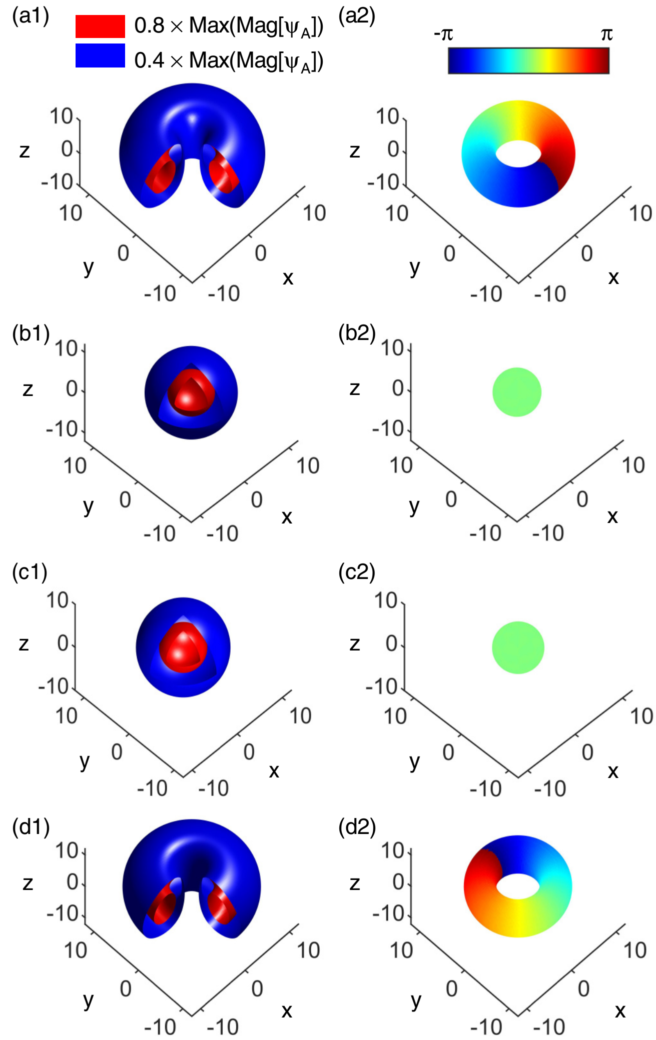

FIG. 2. (a1) Two different isosurfaces and (a2) the phase distribution on the isosurface with $0.8 \times \mathrm{Max}(\mathrm{Mag}[\psi_A])$ of the pseudospin component ψ_A at K. (b1) Isosurfaces and (b2) the phase distribution of the pseudospin component ψ_B at K. (c1) Isosurfaces and (c2) the phase distribution of ψ_A at K'. (d1) Isosurfaces and (d2) the phase distribution of ψ_B at K'. The isosurfaces are plotted with $\omega = 10$ and parts of the isosurfaces are removed for the sake of clarity.

with $l_A = 0$, and the component ψ_B carries a vorticity of $l_B = -1$. Thus, the topological solitons at K and K' both rotate clockwise with a phase difference of π. Note that for a 3D valley-Hall insulator, the topological solitons at K and K' rotate in opposite directions [40].

Existence and stability. In Figs. 3(a) and 3(b), the frequency spectrum is plotted as a function of the powers $P_{A,B}$, which are defined as $P_{A,B} = \int |\psi_{A,B}(\vec{r})|^2 d^3r$. We only show the plots for the topological solitons at K, because the curves for the topological solitoins at K' can be obtained just by replacing $A(B)$ with $B(A)$. The dashed lines indicate the linear band edges. The topological solitons bifurcate from the lower linear band edge with a nonzero P_B, which implies that the topological solitons do not exist below a certain power threshold. The family of topological solitons terminates when the powers

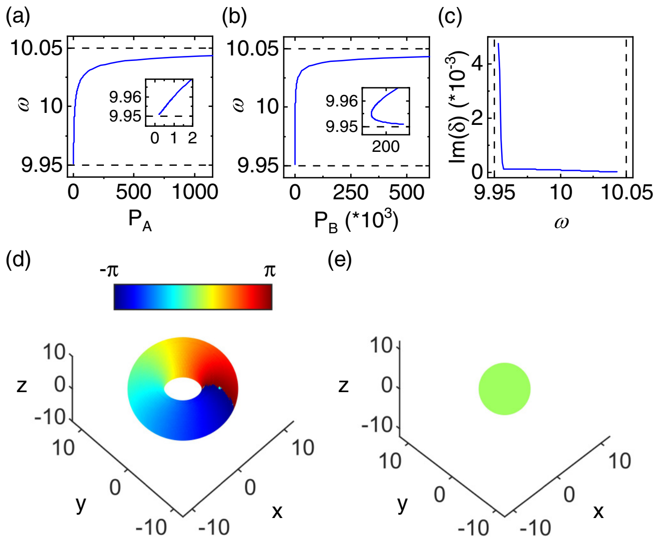

FIG. 3. (a), (b) The power of the two pseudospin components $\psi_{A,B}$. The insets are enlarged figures for $P_{A,B}$. (c) The growth rate $\mathrm{Im}(\delta)$ of the topological solitons. The dashed lines in (a)–(c) denote the linear band edges. (d), (e) The perturbation eigenmode $\tilde{\varepsilon}_A$ and $\tilde{\varepsilon}_B$ at $\omega = 9.953$.

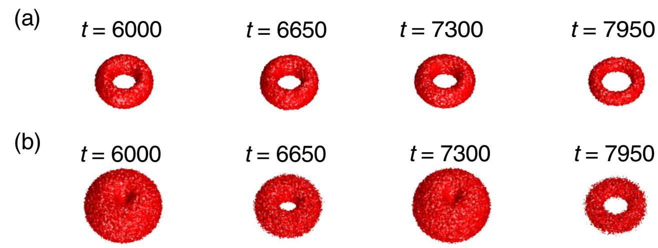

FIG. 4. (a) The isosurfaces with $0.8 \times \mathrm{Max}(\mathrm{Mag}[\psi_A(t=0)])$ of the pseudospin component ψ_A of the stable topological soliton with $\omega = 10$ at K. The four subfigures from left to right correspond to $t = 6000$, 6650, 7300, and 7950, respectively. (b) The isosurfaces with $1.0^*\mathrm{Max}(\mathrm{Mag}[\psi_A(t=0)])$ of ψ_A of the unstable topological soliton with $\omega = 9.953$.

saturate. The power is monotonic within most of the spectrum range. However, near the lower linear band edge, we have $dP_B/d\omega < 0$ [inset of Fig. 3(b)]. This negative slope is related to the stability of the topological solitons.

We study the stability properties of the topological solitons using the linear stability analysis. The solution is sought at the frequency δ in the form of $\psi_{A,B} = (\phi_{A,B} + \varepsilon_{A,B}e^{-i\delta t} + \mu^*_{A,B}e^{i\delta^* t})e^{-i\omega t}$, where $\phi_{A,B}e^{-i\omega t}$ are the unperturbed soliton solutions, and $\varepsilon_{A,B}$ and $\mu_{A,B}$ are the perturbation eigenmodes. Note that the perturbations may come from both the amplitudes and phases. For the perturbation eigenmode with a certain vorticity q, the solution can be written as

$$\begin{pmatrix}\psi_A\\ \psi_B\end{pmatrix} = \left[\begin{pmatrix}\tilde{\phi}_A\\ \tilde{\phi}_B\end{pmatrix} + \begin{pmatrix}\tilde{\varepsilon}_A\\ \tilde{\varepsilon}_B\end{pmatrix}e^{-iq\varphi}e^{-i\delta t} + \begin{pmatrix}\tilde{\mu}^*_A\\ \tilde{\mu}^*_B\end{pmatrix}e^{iq\varphi}e^{i\delta^* t}\right] \times \begin{pmatrix}e^{-i\varphi}\\ 1\end{pmatrix}e^{-i\omega t}. \tag{10}$$

Obviously, the topological solitons are linearly stable if δ is real, whereas they are linearly unstable if the imaginary part of δ, namely the growth rate, is positive. From Fig. 3(c), the topological solitons are linearly stable within most of the spectrum range. At a small regime near the lower linear band edge ($\omega < 9.957$), the topological solitons are linearly unstable because of the emergence of a nonzero imaginary part of δ via a Hopf bifurcation in the $q = 0$ spectrum at $\omega = 9.957$ [Figs. 3(d) and 3(e)]. Such instability is of an exponential nature and can be predicted by the Vakhitov-Kolokolov criterion [44,45], due to the fact that the power P_B dominates the total power and there is a negative slope with $dP_B/d\omega < 0$ near the lower linear band edge [Fig. 3(b)]. This behavior is different from that of the topological solitons in 2D, which are linearly stable near the lower linear band edge [46].

Dynamics. We add $\pm 10\%$ noises with uniform distributions to the topological solitons at K and study their temporal evolution. In Figs. 4(a) and 4(b), we show the isosurfaces of the pseudospin component ψ_A at different times with $\omega = 10$ and $\omega = 9.953$, respectively. For the stable topological soliton with $\omega = 10$, although noises are imposed, the soliton is always self-sustained in all 3D and the radius of the torus tube is invariant [Fig. 4(a)]. For the unstable topological soliton with $\omega = 9.953$, it exhibits a breathing structure [Fig. 4(b)]. The radius of the torus tube and the magnitude of the soliton oscillate along with the temporal evolution. Since the growth rates $\mathrm{Im}(\delta)$ are in the order of 10^{-3}, the topological solitons near the lower linear band edge are weakly unstable. Thus, our topological solitons in 3D should be observable in the whole spectrum range. Furthermore, although the topological solitons are semivortex solitons where the pseudospin component ψ_A has a nonzero vorticity, they are only disturbed by the radially symmetric perturbations with $q = 0$ and radial symmetry breaking is not observed. This behavior agrees with the result from the linear stability analysis.

Conclusion. We find self-localized topological states (i.e., topological solitons) in a 3D nonlinear photonic Chern insulator. The topological solitons at the high-symmetry points K and K' rotate in the same direction, as a manifestation of the topology of the linear host lattice. Specifically, these solitons are stable over a broad frequency range. Because of these features, it is feasible to observe the topological solitons experimentally. Considering that both time-reversal symmetry breaking and nonlinearity can be implemented in electrical circuit lattices [47,48] and 3D circuit lattices are readily available [49], we propose a realistic circuit implementation to observe the topological solitons [40]. Our work establishes how the interplay between topology and nonlinearity leads to a different type of soliton, and can be extended to other 3D topological systems.

Acknowledgments. R.L. was sponsored by the National Natural Science Foundation of China (NSFC) under Grant No. 12104353. P.L. was sponsored by the National Natural Science Foundation of China (NSFC) (11805141), the Applied Basic Research Program of Shanxi Province (201901D211424), and the Scientific and Technological Innovation Programs of Higher Education Institutions in Shanxi (STIP) (2021L401). Y.L. was sponsored by the National Natural Science Foundation of China (NSFC) under Grant No.

61871309 and the 111 Project. The numerical calculations in this paper was supported by High-Performance Computing Platform of Xidian University. Part of the computation is supported by Shenzhen Bkunyun Cloud Computing Co., Ltd.

[1] M. Z. Hasan and C. L. Kane, Colloquium: Topological insulators, Rev. Mod. Phys. **82**, 3045 (2010).
[2] X.-L. Qi and S.-C. Zhang, Topological insulators and superconductors, Rev. Mod. Phys. **83**, 1057 (2011).
[3] A. Kitaev, Periodic table for topological insulators and superconductors, in *Advances in Theoretical Physics: Landau Memorial Conference*, edited by V. Lebedev and M. Feigel'man, AIP Conf. Proc. Vol. 1134 (AIP, Melville, NY, 2009), p. 22.
[4] S. Ryu, A. P. Schnyder, A. Furusaki, and A. W. W. Ludwig, Topological insulators and superconductors: tenfold way and dimensional hierarchy, New J. Phys. **12**, 065010 (2010).
[5] K. Shiozaki and M. Sato, Topology of crystalline insulators and superconductors, Phys. Rev. B. **90**, 165114 (2014).
[6] N. P. Armitage, E. J. Mele, and A. Vishwanath, Weyl and Dirac semimetals in three-dimensional solids, Rev. Mod. Phys. **90**, 015001 (2018).
[7] J. Xiao and B. Yan, First-principles calculations for topological quantum materials, Nat. Rev. Phys. **3**, 283 (2021).
[8] L. Lu, C. Fang, L. Fu, S. G. Johnson, J. D. Joannopoulos, and M. Soljačić, Symmetry-protected topological photonic crystal in three dimensions, Nat. Phys. **12**, 337 (2016).
[9] A. Slobozhanyuk, S. H. Mousavi, X. Ni, D. Smirnova, Y. S. Kivshar, and A. B. Khanikaev, Three-dimensional all-dielectric photonic topological insulator, Nat. Photonics **11**, 130 (2017).
[10] Y. Yang, Z. Gao, H. Xue, L. Zhang, M. He, Z. Yang, R. Singh, Y. Chong, B. Zhang, and H. Chen, Realization of a three-dimensional photonic topological insulator, Nature (London) **565**, 622 (2019).
[11] C. He, H.-S. Lai, B. He, S.-Y. Yu, X. Xu, M.-H. Lu, and Y.-F. Chen, Acoustic analogues of three-dimensional topological insulators, Nat. Commun. **11**, 2318 (2020).
[12] D. Wang, B. Yang, W. Gao, H. Jia, Q. Yang, X. Chen, M. Wei, C. Liu, M. Navarro-Cía, J. Han, W. Zhang, and S. Zhang, Photonic Weyl points due to broken time-reversal symmetry in magnetized semiconductor, Nat. Phys. **15**, 1150 (2019).
[13] F. Li, X. Huang, J. Lu, J. Ma, and Z. Liu, Weyl points and Fermi arcs in a chiral phononic crystal, Nat. Phys. **14**, 30 (2018).
[14] M. Xiao, W.-J. Chen, W.-Y. He, and C. T. Chan, Synthetic gauge flux and Weyl points in acoustic systems, Nat. Phys. **11**, 920 (2015).
[15] L. Lu, Z. Wang, D. Ye, L. Ran, L. Fu, J. D. Joannopoulos, and M. Soljačić, Experimental observation of Weyl points, Science **349**, 622 (2015).
[16] J. Noh, S. Huang, D. Leykam, Y. D. Chong, K. P. Chen, and M. C. Rechtsman, Experimental observation of optical Weyl points and Fermi arc-like surface states, Nat. Phys. **13**, 611 (2017).
[17] Y. S. Kivshar and G. P. Agrawal, *Optical Solitons: From Fibers to Photonic Crystals* (Academic, Boston, 2003).
[18] D. Smirnova, D. Leykam, Y. Chong, and Y. Kivshar, Nonlinear topological photonics, Appl. Phys. Rev. **7**, 021306 (2020).
[19] D. Leykam and Y. D. Chong, Edge Solitons in Nonlinear-Photonic Topological Insulators, Phys. Rev. Lett. **117**, 143901 (2016).
[20] Y. V. Kartashov, A. A. Arkhipova, S. A. Zhuravitskii, N. N. Skryabin, I. V. Dyakonov, A. A. Kalinkin, S. P. Kulik, V. O. Kompanets, S. V. Chekalin, L. Torner, and V. N. Zadkov, Observation of Edge Solitons in Topological Trimer Arrays, Phys. Rev. Lett. **128**, 093901 (2022).
[21] S. Mukherjee and M. C. Rechtsman, Observation of Unidirectional Solitonlike Edge States in Nonlinear Floquet Topological Insulators, Phys. Rev. X **11**, 041057 (2021).
[22] O. Bleu, G. Malpuech, and D. D. Solnyshkov, Robust quantum valley Hall effect for vortices in an interacting bosonic quantum fluid, Nat. Commun. **9**, 3991 (2018).
[23] Z. Zhang, R. Wang, Y. Zhang, Y. V. Kartashov, F. Li, H. Zhong, H. Guan, K. Gao, F. Li, Y. Zhang, and M. Xiao, Observation of edge solitons in photonic graphene, Nat. Commun. **11**, 1902 (2020).
[24] S. K. Ivanov, Y. V. Kartashov, M. Heinrich, A. Szameit, L. Torner, and V. V. Konotop, Topological dipole Floquet solitons, Phys. Rev. A **103**, 053507 (2021).
[25] W. Zhang, X. Chen, Y. V. Kartashov, V. V. Konotop, and F. Ye, Coupling of Edge States and Topological Bragg Solitons, Phys. Rev. Lett. **123**, 254103 (2019).
[26] Y. Lumer, Y. Plotnik, M. C. Rechtsman, and M. Segev, Self-Localized States in Photonic Topological Insulators, Phys. Rev. Lett. **111**, 243905 (2013).
[27] S. Mukherjee and M. C. Rechtsman, Observation of Floquet solitons in a topological bandgap, Science **368**, 856 (2020).
[28] D. A. Smirnova, L. A. Smirnov, D. Leykam, and Y. S. Kivshar, Topological edge states and gap solitons in the nonlinear Dirac model, Laser Photonics Rev. **13**, 1900223 (2019).
[29] A. N. Poddubny and D. A. Smirnova, Ring Dirac solitons in nonlinear topological systems, Phys. Rev. A **98**, 013827 (2018).
[30] D. D. Solnyshkov, O. Bleu, B. Teklu, and G. Malpuech, Chirality of Topological Gap Solitons in Bosonic Dimer Chains. Phys. Rev. Lett. **118**, 023901 (2017).
[31] J. L. Marzuola, M. Rechtsman, B. Osting, and M. Bandres, Bulk soliton dynamics in bosonic topological insulators, arXiv:1904.10312.
[32] V. Pardo and W. E. Pickett, Half-Metallic Semi-Dirac-Point Generated by Quantum Confinement in TiO_2/VO_2 Nanostructures, Phys. Rev. Lett. **102**, 166803 (2009).
[33] C. He, S.-Y. Yu, H. Wang, H. Ge, J. Ruan, H. Zhang, M.-H. Lu, and Y.-F. Chen, Hybrid Acoustic Topological Insulator in Three Dimensions, Phys. Rev. Lett. **123**, 195503 (2019).
[34] N. Mohanta, J. M. Ok, J. Zhang, H. Miao, E. Dagotto, H. N. Lee, and S. Okamoto, Semi-Dirac and Weyl fermions in transition metal oxides, Phys. Rev. B **104**, 235121 (2021).
[35] G.-G. Liu, P. Zhou, Y. Yang, H. Xue, X. Ren, X. Lin, H. Sun, L. Bi, Y. Chong, and B. Zhang, Observation of an unpaired photonic Dirac point, Nat. Commun. **11**, 1873 (2020).
[36] J. Cuevas-Maraver, P. G. Kevrekidis, A. Saxena, A. Comech, and R. Lan, Stability of Solitary Waves and Vortices in a 2D Nonlinear Dirac Model, Phys. Rev. Lett. **116**, 214101 (2016).

[37] J. Cuevas-Maraver, P. G. Kevrekidis, F. G. Mertens, and A. Saxena, Speed-of-light pulses in a massless nonlinear Dirac equation, Phys. Rev. E **100**, 022210 (2019).

[38] F. D. M. Haldane, Model for a Quantum Hall Effect without Landau Levels: Condensed-Matter Realization of the "Parity Anomaly", Phys. Rev. Lett. **61**, 2015 (1988).

[39] G.-G. Liu, Z. Gao, P. Zhou, Q. Wang, Y.-H. Hu, M. Wang, C. Liu, X. Lin, S. A. Yang, Y. Yang, Y. Chong, and B. Zhang, Observation of Weyl point pair annihilation in a gyromagnetic photonic crystal, arXiv:2106.02461.

[40] See Supplemental Material at http://link.aps.org/supplemental/10.1103/PhysRevB.105.L201111 for detailed discussions of the coupled equations for the 3D photonic Chern insulator, topological solitons in a 3D valley-Hall insulator, topological solitons under a self-defocusing nonlinearity, and circuit realization of the topological solitons.

[41] Y. V. Kartashov, L. Torner, M. Modugno, E. Ya. Sherman, B. A. Malomed, and V. V. Konotop, Multidimensional hybrid Bose-Einstein condensates stabilized by lower-dimensional spin-orbit coupling, Phys. Rev. Research **2**, 013036 (2020).

[42] Y. V. Kartashov, G. E. Astrakharchik, B. A. Malomed, and L. Torner, New frontiers in multidimensional self-trapping of nonlinear fields and matter, Nat. Rev. Phys. **1**, 185 (2019).

[43] R. Y. Chiao, E. Garmire, and C. H. Townes, Self-Trapping of Optical Beams, Phys. Rev. Lett. **13**, 479 (1964).

[44] N. G. Vakhitov and A. A. Kolokolov, Stationary solutions of the wave equation in the medium with nonlinearity saturation, Radiophys. Quantum Electron. **16**, 783 (1973).

[45] E. A. Kuznetsov, A. M. Rubenchik, and V. E. Zakharov, Soliton stability in plasmas and hydrodynamics, Phys. Rep. **142**, 103 (1986).

[46] J. Cuevas-Maraver, P. G. Kevrekidis, A. B. Aceves, and A. Saxena, Solitary waves in a two-dimensional nonlinear Dirac equation: from discrete to continuum, J. Phys. A: Math. Theor. **50**, 495207 (2017).

[47] T. Hofmann, T. Helbig, C. H. Lee, M. Greiter, and R. Thomale, Chiral Voltage Propagation and Calibration in a Topolectrical Chern Circuit, Phys. Rev. Lett. **122**, 247702 (2019).

[48] Y. Hadad, J. C. Soric, A. B. Khanikaev, and A. Alù, Self-induced topological protection in nonlinear circuit arrays, Nat. Electron. **1**, 178 (2018).

[49] R. Li, B. Lv, H. Tao, J. Shi, Y. Chong, B. Zhang, and H. Chen, Ideal type-II Weyl points in topological circuits, Natl. Sci. Rev. **8**, nwaa192 (2021).